SB4: Integrated Photonics

Final Report

Lucas Ng*

13th June 2025

1 Introduction

In the first interim report, we performed modal analysis on a symmetric planar waveguide of several core and cladding materials, with further investigation into the effects of waveguide geometry and modal excitation wavelength on the modal properties, including the effective index, group index, birefringence, and dispersion characteristics.

The second interim report recognised that waveguides do not exist in isolation, and presented the coupled mode theory as a framework for understanding the power transfer across coupled waveguides, with a derivation via considering the coupled mode propagation matrix,

$$\mathbf{M} = \begin{pmatrix} \beta & \kappa \\ \kappa & \beta \end{pmatrix},$$

to be the infinitessimal generator matrix that generates the modal evolution transition matrix as a one-parameter subgroup of the Lie group $GL(2, \mathbb{C})$ via the exponential map $-jzM \mapsto e^{-jzM}$ (where z is the propagation distance along the waveguide) that acts on an element of the Lie algebra $\mathfrak{gl}(2, \mathbb{C})$. This formalism demonstrated how the intrinsic structure of M gives rise to the modal properties of the coupled waveguide: the symmetry of the matrix M corresponds to reciprocal coupling, while real-valued β and κ encodes the conservation of power in the coupled waveguide, since in this instance, $-jzM$ is Hermitian, and thus the image of the exponential map is unitary.

Likewise, this current, final report, ascends to the next level of abstraction, *á la mise en abyme*, considering the whole structure of a S-bend directional coupler in its entirety. At this level, the previous theoretical frameworks serve purely as approximation, and we must account for bending losses, asymmetric couplers, and other practical and interesting considerations. This being analytically intractable, Lumerical's FDTD software[1] was utilised to simulate the directional coupler.

*ln373@cam.ac.uk

1. *FDTD Solution: 3D Electromagnetic Simulator* (Vancouver, Canada: Lumerical Inc.), https://www.lumerical.com.

2 Simulation setup

The geometry of our directional coupler is the traditional doubly-symmetric S-bend design, with a parallel coupling length connected in each waveguide to its input and output ports by S-bends. Each port is extended by a straight waveguide which extends through to 1 μm outside the FDTD simulation region, which is otherwise internally padded on all sides by 2.5 μm of perfectly matched layer (PML) boundary conditions. The input port of the upper waveguide is excited by a modal source at the wavelength of interest.

This form of the directional coupler is, by way of metaphor, structured as an aubade. Figure 1 shows how the geometry is parameterised by the widths of each waveguide (which may be varied independently), the separation gap between the two waveguides, the length of the coupling region, and the wavelength of the modal source. The waveguide material is silicon with a cladding of silicon dioxide, with wavelength-dependent refractive indices taken from the `Si (Silicon) - Palik` and `SiO2 (Glass) - Palik` entries of the Lumerical material database respectively. The waveguide depth into the plane is 220 nm for both waveguides, the ports on each end are separated by 10 μm in the horizontal direction, and the poles of the S-bends are placed at $[(0,0),(\pm 5,0),(\pm 5,\mp 5),(\pm 5,\mp 5)]$ μm. The TE_0 mode is launched at the input port.

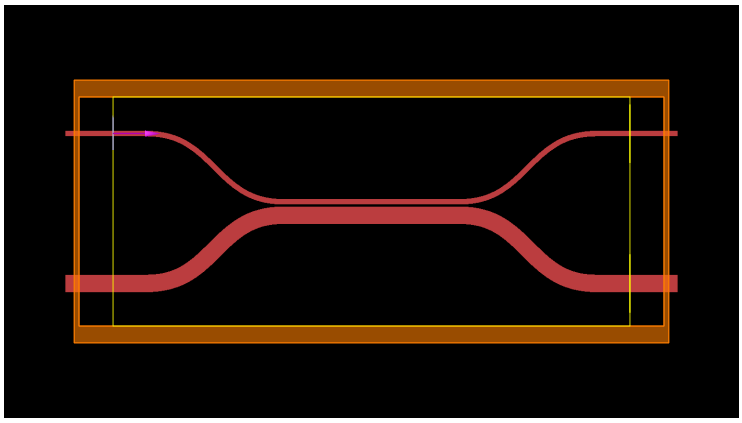

Figure 1: Schematic of the S-bend directional coupler geometry with parameters $w_1 = 400$ nm, $w_2 = 1280$ nm, separation = 150 nm, and $L = 13.0$ μm.

3 Results

3.1 TE_0-TE_0 coupling

For equal waveguide widths, it is quite straightforward to achieve arbitrary TE_0-TE_0 power transfer between the two coupled waveguides. With TE_0 launched at the input port of the upper waveguide, a co-located waveguide symmetrised across the separation gap supports TE_0 at the same effective index (subject to fabrication tolerances), and thus the TE_0 mode is coupled to the TE_0 mode of the lower waveguide.

Other modes have a large phase mismatch $\Delta\beta = k_0 \Delta n_{\text{eff}} \gg 1$ with respect to TE_0, and hence cross-mode leakage has a negligible modal power beating amplitude of

$$A \propto \frac{\kappa^2}{\kappa^2 + \left(\frac{\Delta\beta}{2}\right)^2} \approx \left(\frac{2\kappa}{\Delta\beta}\right)^2 \to 0.$$

Moreover, by selecting the waveguide width to be sufficiently small, higher order modes can be suppressed, as they are not supported by the waveguide geometry.

The proportion of the power transferred to the lower waveguide is then a function of the coupling length L,

$$P \propto \sin^2\left(\frac{\kappa L}{2}\right),$$

where κ is the coupling coefficient, which is a function of the waveguide geometry and the wavelength of the modal source.

Power transfer as a function of coupling length Figure 2 shows the power transfer as a function of the coupling length L for a fixed waveguide width of 500 nm and separation gap of 150 nm, with the TE_0 mode launched at a wavelength of 1550 nm from the input port of the upper waveguide. The coupled mode theory predicts sinusoidal power beating, with half-power transfer to occur at a minimum coupling length of $L_{3\text{db}} = \frac{\pi}{4\kappa}$, and for total power transfer to occur at a minimum coupling length $L_c = \frac{\pi}{2\kappa}$. Indeed, we observe $\hat{L}_{3\text{db}} \approx 10\,\mu\text{m}$ and $\hat{L}_c \approx 21\,\mu\text{m}$ in the simulation results. This implies a coupling coefficient of $\hat{\kappa} \approx 0.4\,\mu\text{m}^{-1}$.

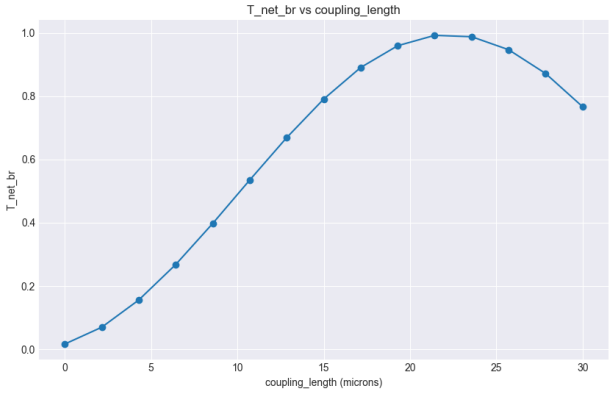

Figure 2: Cross-power transfer fraction at the coupled output port as a function of coupling length L for a fixed waveguide width of 500 nm and separation gap of 150 nm under input port TE_0 mode excitation at 1550 nm.

Half-power transfer Figure 3 shows the power intensity distribution across the waveguide plane for the half-power simulation at $\hat{L}_{3\text{db}} \approx 10\,\mu\text{m}$. The TE_0 mode monitor registers a power transfer fraction of 0.5056 while the lower waveguide TE_0 mode monitor registers a power transfer fraction of 0.4895. This implies some power loss, but higher-order mode monitors show that either the mode is not supported, or that the power transfer fraction is negligible.

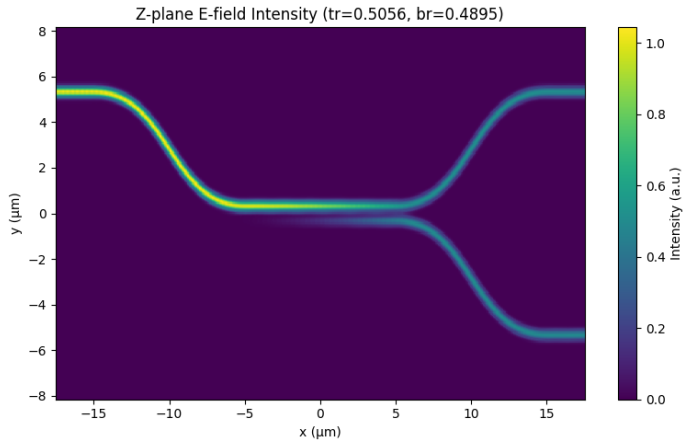

Figure 3: Power intensity distribution across the waveguide plane at the half-power coupling length $\hat{L}_{3\text{db}} \approx 10\,\mu\text{m}$ for a fixed waveguide width of 500 nm and separation gap of 150 nm under input port TE_0 mode excitation at 1550 nm.

Total power transfer Figure 4 shows the power intensity distribution across the waveguide plane for the total power transfer simulation at $\hat{L}_c \approx 21\,\mu\text{m}$. With cross-mode power transfer to the lower waveguide TE_0 mode monitor registering a power transfer fraction of 0.9920, we can conclude that the upper TE_0 mode is indeed coupled strongly to the lower waveguide TE_0 mode. This latter parameter set gives us an optimised directional coupler operating at $\lambda = 1550\,\text{nm}$.

It should be noted that such a small separation gap utilised above is the minimum of what is achievable in practice, and in the next section we will explore the effect of varying the separation gap on the power transfer fraction.

Optimising for a shorter wavelength To additionally optimise a directional coupler for a shorter wavelength $\lambda = 1310\,\text{nm}$, we could repeat the above procedure with the same fixed waveguide width of 500 nm and separation gap of 150 nm. However, a shorter wavelength requires a larger coupling length to achieve the same fraction of power transfer.

Figure 5 shows the power transfer as a function of the coupling length L for a fixed waveguide width of 500 nm and separation gap of 150 nm over the same swept range as before, and within this range, we cannot even achieve half-power transfer, let alone total power transfer. It seems that either we need to have a very large coupling length, or to modify the waveguide geometry.

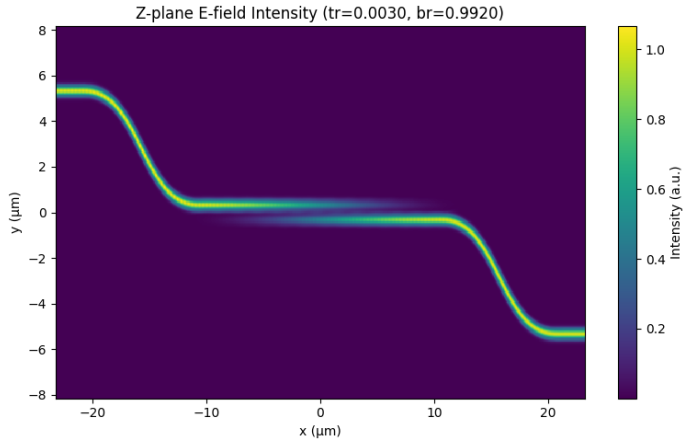

Figure 4: Power intensity distribution across the waveguide plane at the total power transfer coupling length $\hat{L}_c \approx 21\,\mu$m for a fixed waveguide width of 500 nm and separation gap of 150 nm under input port TE_0 mode excitation at 1550 nm.

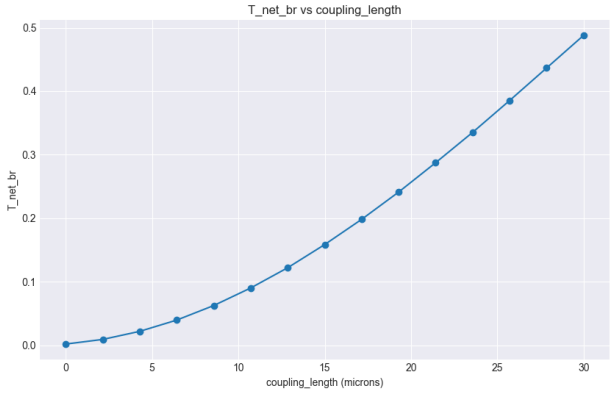

Figure 5: Cross-power transfer fraction at the coupled output port as a function of coupling length L for a fixed waveguide width of 500 nm and separation gap of 150 nm under input port TE_0 mode excitation at 1310 nm.

Reducing the coupling length Assuming fabrication tolerances are not a concern and we do not require the dimensions of the directional coupler to match other components in the photonic circuit, like cascaded couplers or integrated Michelson interferometers, it is desireable to reduce the coupling length.

Shorter directional couplers have a smaller footprint, less propagation loss and latency, and support a broader spectral bandwidth. Additionally they are more robust against accumulated phase mismatch arising from non-idealities in the fabrication process.

One strategy to achieve this for our directional coupler at $\lambda = 1310$ nm is to use the fact that decreasing the waveguide width increases the lateral evanescent extent of the modes, which in turn increases the coupling coefficient κ and thus

decreases the coupling length $L_c = \frac{\pi}{2\kappa}$.

By reducing the waveguide width to 400 nm, we can achieve Figure 6, which shows that we can achieve half-power transfer at $\hat{L}_{3\text{db}} \approx 11\,\mu\text{m}$ and total power transfer at $\hat{L}_c \approx 23\,\mu\text{m}$. This is much more comparable to the $\hat{L}_{3\text{db}} \approx 10\,\mu\text{m}$ and $\hat{L}_c \approx 21\,\mu\text{m}$ for the 1550 nm wavelength case with a 500 nm waveguide width.

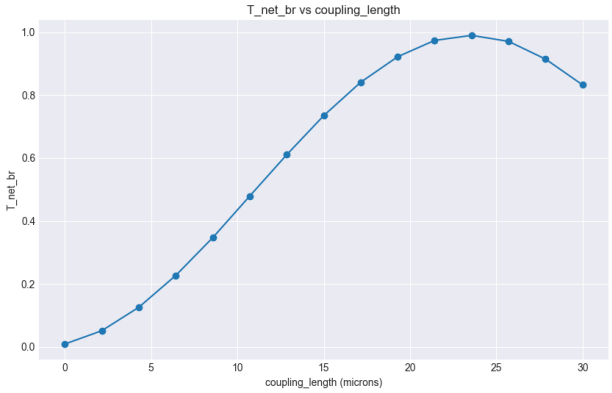

Figure 6: Cross-power transfer fraction at the coupled output port as a function of coupling length L for a fixed waveguide width of 400 nm and separation gap of 150 nm under input port TE_0 mode excitation at 1310 nm.

3.2 Effect of waveguide width and separation gap

It is not always so trivial to design a directional coupler that achieves the desired operation characteristics, hence it is useful to explore the effect of the hyperparameters fixed before optimised over the coupling length L, namely the waveguide width and separation gap.

Figure 7 shows the power transfer fraction to the lower waveguide TE_0 mode monitor as a function of the uniform waveguide width w swepth through $w \in [0.1, 1.0]\,\mu\text{m}$ and separation gap s swept through $s \in [0.15, 0.5]\,\mu\text{m}$ for a fixed coupling length of $10\,\mu\text{m}$ and input port TE_0 mode excitation at 1550 nm. For the majority of the parameter space, there is very weak coupling. However, we observe a ridge of strong power transfer along the entire separation axis at a waveguide width of $w = 0.36\,\mu\text{m}$, with a peak at $s = 0.25\,\mu\text{m}$.

Effect of waveguide width While a small waveguide width increases the evanescent overlap, it also reduces the mode confinement and increases propagation losses, hence there are very high bending-induced radiative losses for small waveguide widths. Figure 8 shows the power intensity distribution across the waveguide plane for a waveguide width just before the ridge $w = 0.23\,\mu\text{m}$ and at the optimal separation gap $s = 0.25\,\mu\text{m}$.

From this it is clear that the mode is not well confined, and loses almost all of its power along the input port S-bend.

Very large waveguide widths, on the other hand, have much stronger mode confinement, with a smaller evanescent tail, which reduces the coupling coeffi-

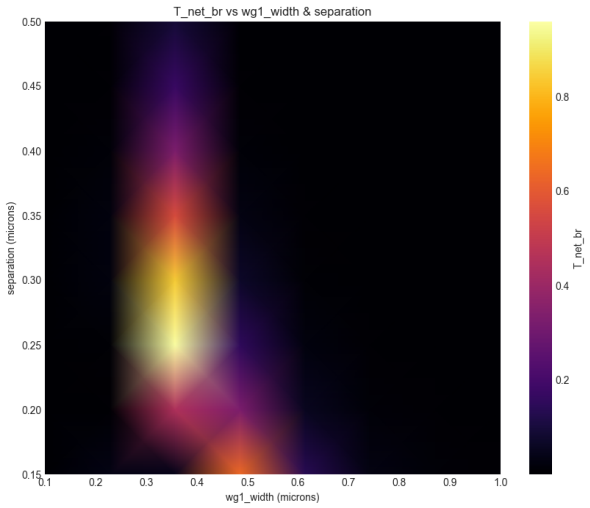

Figure 7: Cross-power transfer fraction at the coupled output port as a function of waveguide width w and separation gap s for a fixed coupling length of $10\,\mu$m under input port TE_0 mode excitation at 1550 nm.

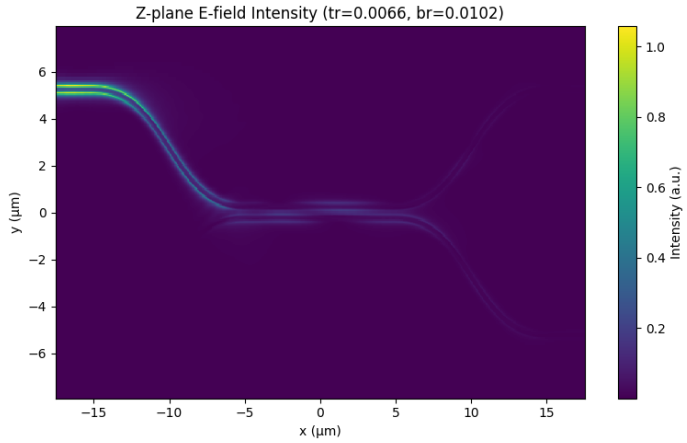

Figure 8: Power intensity distribution across the waveguide plane at the coupling length $L = 10\,\mu$m for a waveguide width of $w = 0.23\,\mu$m and separation gap of $s = 0.25\,\mu$m under input port TE_0 mode excitation at 1550 nm.

cient κ and thus the power transfer fraction. (You could increase the coupling length L to compensate for this, in this plot it was held as constant.) The optimal waveguide width is thus a balance between these two effects, and the ridge of strong power transfer at $w = 0.36\,\mu$m is the result of this trade-off.

Effect of separation gap Now that we have established the optimal waveguide width, in analysis of the separation gap, it may be more intuitive to fix the width at this optimum and consider effect of separation on the ridge profile, which is shown in Figure 9. At a large separation, the power transfer fraction decays exponentially, but at a small separation, the power transfer fraction is also small and increases linearly with the separation gap.

The former can be rationalised by the fact that the evanescent tails of the modes in each waveguide overlap less and less as the separation gap increases. However, the latter is less intuitive. At very small separation, the two-waveguide supermodes are heavily hybridized; effective indices split strongly, resulting in a large coupling coefficient κ. However, since the coupling length L is fixed, the output phase of the power beating is not optimised for maximum cross-power transfer. Indeed, Figure 7 show that, for very small separations, the ridge of strong cross-power transfer moves diagonally towards larger waveguide widths. Since increasing the waveguide width decreases the coupling coefficient κ by reducing the degree of hybridization, these two effects cancel out, and the power transfer fraction remains optimised at the fixed coupling length L.

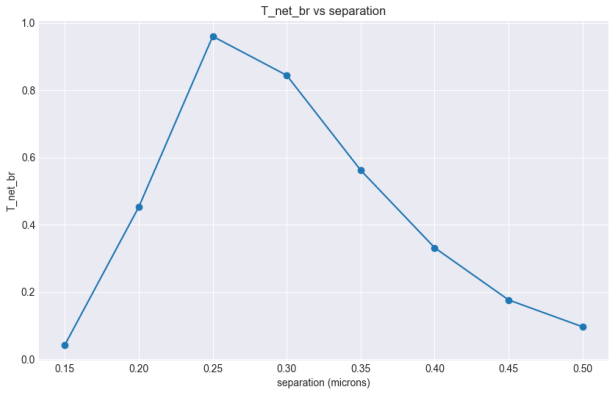

Figure 9: Cross-power transfer fraction at the coupled output port as a function of separation gap s for a fixed waveguide width of $w = 0.36\,\mu$m under input port TE_0 mode excitation at 1550 nm.

3.3 Cross-order mode coupling

Designing for coupling across modes of different orders is less trivial. For the TE_0-TE_0 case we were able to rely on the fact that equal waveguide widths impose TE_0 phase matching across the separation gap, but this is not the case for general cross-order mode coupling.

There is an additional step of design required to achieve cross-order mode coupling: matching the effective indices of the two modes across the separation gap.

TE_0-TE_2 coupling Let us consider the example of designing a directional coupler that transfers maximum power from the TE_0 mode of the upper waveg-

uide to the TE_2 mode of the lower waveguide. Recall Figure 10 from the first interim report.[2] This idealised planar case demonstrates that we expect that, with the upper waveguide width fixed at $w_1 = 0.4\,\mu$m, we expect it to be able to couple to the TE_2 mode of the lower waveguide when it is at a width $1 < w_2 \leq 1.5$.

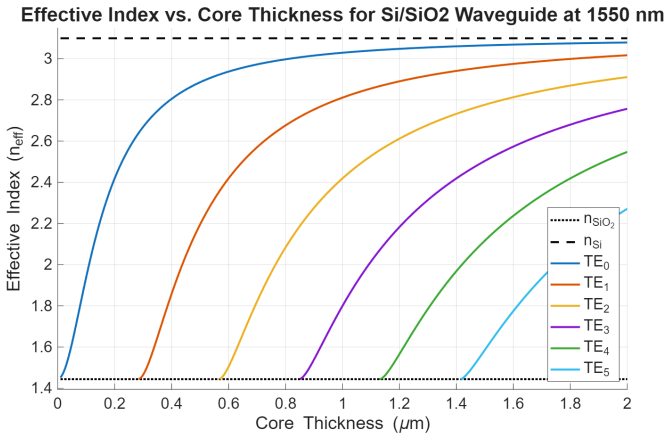

Figure 10: Effective indices of TE_0-TE_5 as a function of waveguide thickness.

To avoid adding additional monitors to the simulation sweep, it will suffice to use the upper output port TE_0 mode monitor as an inverse proxy for the lower output port TE_2 mode monitor. One design strategy is to sweep both the lower waveguide width w_2 through the range $w_2 \in (1, 1.5]\,\mu$m and the coupling length $L \in [10, 40]\,\mu$m while keeping the separation gap fixed at $s = 0.15\,\mu$m. This produces the heatmap in Figure 11 of the power fraction received by the proxy TE_0 mode monitor on the upper waveguide.

Clearly, we have a sinusoidal ridge of recorded power transfer along the coupling length axis, at a waveguide width of $w_2 = 1.28\,\mu$m. Fixing that width and looking along at ridge results in Figure 12, showing the optimum coupling length L for maximum power transfer to the TE_2 mode of the lower waveguide to be $\hat{L} \approx 13\,\mu$m. Figure 13 shows the power intensity distribution across the waveguide plane at this coupling length, with the TE_0 mode monitor on the upper waveguide registering a power transfer fraction of 0.0182 and the TE_2 mode monitor on the lower waveguide registering a power transfer fraction of 0.9235. This means the TE_2 mode is excited to 98.1% of the total power fraction it shares with the TE_0 mode at the input port of the upper waveguide. There is some launched power unaccounted for, but that can be assigned to modal leakage.

This is the directional coupler shown originally in Figure 1.

2. Lucas Ng, "SB4: Integrated Photonics - 1st Interim Report," May 23, 2025,

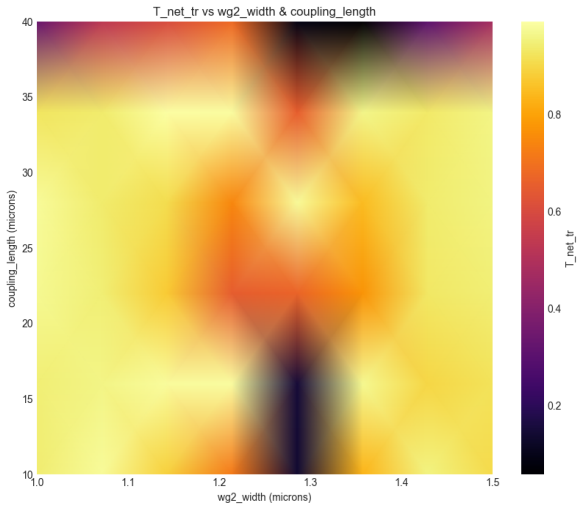

Figure 11: Cross-power transfer fraction at the upper waveguide TE_0 mode monitor as a function of lower waveguide width w_2 and coupling length L for a fixed upper waveguide width of $w_1 = 0.4\,\mu$m and separation gap of $s = 0.15\,\mu$m under input port TE_0 mode excitation at 1550 nm.

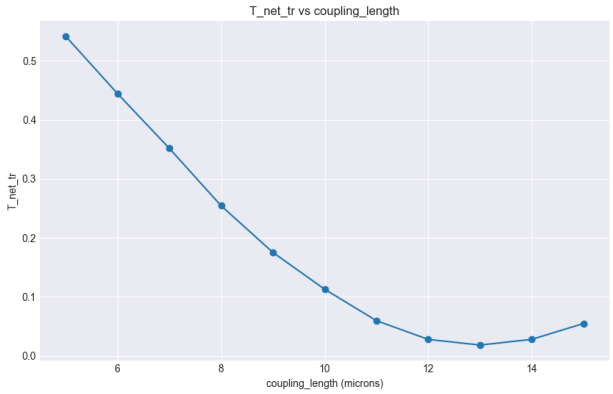

Figure 12: Power transfer fraction at the upper waveguide TE_0 mode monitor as a function of coupling length L for a fixed upper waveguide width of $w_1 = 0.4\,\mu$m, lower waveguide width of $w_2 = 1.28\,\mu$m, and separation gap of $s = 0.15\,\mu$m under input port TE_0 mode excitation at 1550 nm.

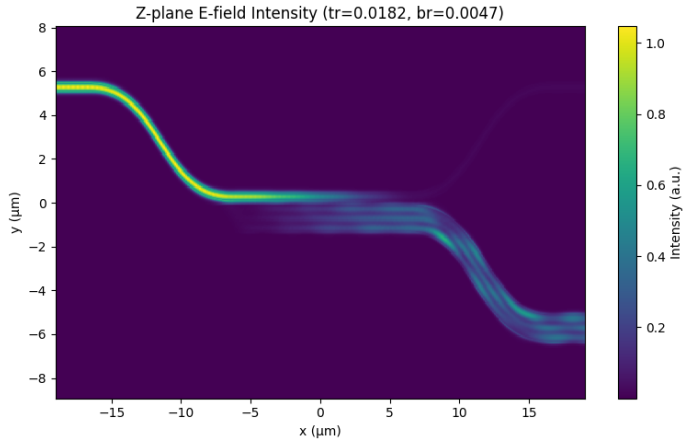

Figure 13: Power intensity distribution across the waveguide plane at the coupling length $L = \hat{L} \approx 13\,\mu$m for a fixed upper waveguide width of $w_1 = 0.4\,\mu$m, lower waveguide width of $w_2 = 1.28\,\mu$m, and separation gap of $s = 0.15\,\mu$m under input port TE_0 mode excitation at 1550 nm.

4 Other contributions

5 Conclusion

References

Lumerical Inc. *FDTD Solution: 3D Electromagnetic Simulator*. Vancouver, Canada: Lumerical Inc. https://www.lumerical.com.

Ng, Lucas. "SB4: Integrated Photonics - 1st Interim Report," May 23, 2025.